ELSEVIER

Intermetallics 9 (2001) 581–589

Intermetallics

www.elsevier.com/locate/intermet

Synthesis of nickel–aluminide foams by pack-aluminization of nickel foams

A.M. Hodge*, D.C. Dunand

Department of Materials Science and Engineering, Northwestern University, Evanston, IL 60208, USA

Received 22 February 2001; accepted 9 May 2001

Abstract

Nickel–aluminide foams were synthesized from unalloyed nickel foams by using a two-step, high-activity pack-aluminizing process at 1273 K. After processing, the nickel–aluminide foams exhibited the original structure of the original nickel foams (open-cells with hollows struts and low density). Single-phase NiAl foams, with average composition within 1 wt.% of stoichiometry and with 92% open porosity, were produced by first selecting the appropriate aluminizing time, and then annealing to homogenize the structure. Foams of average Ni_3Al composition were produced by the same method, but multiple intermetallic phases remained due to large variations in strut thickness and thus local composition. Nickel wires and tubes were also aluminized at 1273 K and homogenized for different times to further investigate the aluminizing kinetics and the creation of Kirkendall pores. For aluminization depths up to about 100 μm, Kirkendall pores can be avoided, leading to pore-free struts in the foam.

Keywords: A. Nickel aluminides, based on NiAl; A. Nickel aluminides, based on Ni_3Al; C. Coatings, intermetallic and otherwise; C. Heat treatment; C. Vapour deposition

1. Introduction

Metallic foams exhibit low density and high specific strength, stiffness and surface area, which make them attractive for acoustic and thermal insulation use and for structural applications such as sandwich panels [1]. Developing an intermetallic foam with high melting temperature, high creep strength and good corrosion- and oxidation resistance would allow many novel applications at elevated temperatures [2], e.g. as foam-filled cores of insulating sandwich panels for aerospace skins or engine casings, or as a core within hollow gas turbine blades. A nickel–aluminide foam would be particularly interesting, as NiAl and Ni_3Al in bulk form have been the subject of extensive research over the last decades and have sparked interest for many high-temperature applications [3,4]. Traditional liquid-phase methods for processing metal foams, when applied to nickel aluminides, present severe challenges due to the high melting temperatures and high reactivity of the melt. Alternatively, solid-state techniques can be used, as shown by Chung et al. [5] who pack-aluminized a partially-sintered nickel anode into porous NiAl. Self-propagating high-temperature synthesis of nickel aluminides from elemental powders can also result in porous NiAl and Ni_3Al [6]. However, for both of the above methods, the shape, size, spacing and connectivity of the pores is difficult to control and the porosity achieved is much lower than typically associated with foams. To our knowledge, no highly-ordered, cellular intermetallic foams have been produced by any method to date.

Starting with a cellular nickel foam (which can be produced, e.g. by nickel deposition in the liquid or gas phase upon a sacrificial polymer foam), we investigate in the present paper the fabrication of a nickel-aluminide foam by pack aluminization. This method has been extensively used in the past to provide protective coatings on nickel and nickel-base superalloys, as it creates a corrosion-, oxidation- and temperature-resistant intermetallic layer of NiAl or Ni_3Al. The kinetics and thermodynamics of layer aluminization have been discussed elsewhere [7–10]. Previous research on pack aluminization focused on aluminide surface layers used as coatings, which were much thinner than the substrate. In contrast,

* Corresponding author. Fax: +1-847-491-7820.
E-mail address: a-pulgarin@northwestern.edu (A.M. Hodge).

0966-9795/01/$ - see front matter
PII: S0966-9795(01)00047-4

we investigate in the present paper the complete conversion of nickel to nickel–aluminide specimens by pack-aluminization. Furthermore, we focus specifically on the complex geometry of open-cell foams.

2. Experimental procedures

2.1. Initial nickel foams

Two unalloyed nickel foams (>99.0% purity) were used: a coarse foam with 20 ppi (pores per linear inch) from Astro Met (Cincinnati, OH), fabricated by reduction of nickel oxide [11], and a finer foam with 80 ppi from Goodfellow (Cambridge, UK) made by Chemical Vapor Deposition (CVD) [12]. The foams span a range of relative densities (ratio of foam density and solid density) and geometric parameters (cell size, strut width, strut wall thickness), as presented in Table 1. Scanning electron microscope (SEM) micrographs were used to measure the cell geometric parameters. Foam density was determined from mass and volume measurements.

2.2. Aluminization process

To produce NiAl foams, a high-activity, two-step pack-aluminizing process was chosen, as described for the formation of aluminide layers on bulk nickel [7–10,13]. The aluminum source in the pack determines the activity of the pack [13] where an aluminum content $\geqslant$60 at.% Al is generally considered a high-activity pack. The pack consisted of 3 wt.% NH_4Cl activator from Fisher Scientific (Pittsburgh, PA), 15 wt.% Al (99.8% pure, $-40+325$ mesh) from Alfa Aesar (Ward Hill, MA), and 82 wt.% Al_2O_3 powder filler from C-E Minerals (Baton Rouge, LA). A total pack mass of 25 g was contained in a nickel crucible with 75 ml capacity, covered with a high-chromium stainless-steel sheet. The nickel foam (mass ranging from 0.21 to 0.26 g. for the 80 ppi foam and 0.33 to 0.44 g for the 20 ppi foam) was embedded within a layer of pure Al_2O_3 powder which extended 2 mm above and below the foam and was located midway within the pack. This arrangement prevented direct contact between the nickel foam and the aluminum powders in the pack, which was found to result in a highly exothermic reaction leading to localized melting of the nickel struts.

Aluminization was conducted under an argon atmosphere with the crucible initially placed in the water-cooled end of a vertical tube furnace (700 mm in length) and subsequently rapidly raised into the hot zone of the furnace. The aluminization process was carried out at 1273−5 K for times ranging from 10 min to 4 h, after which the crucible was rapidly lowered back to the water-cooled end and allowed to cool to room temperature under argon. Because it was found that the pack was exhausted after about 5 h at 1273 K, longer aluminization times were not investigated.

To determine the kinetics of aluminization for more simple geometries, aluminization experiments were also conducted on nickel tubes and wires. The nickel wires (99.99% purity, from Alfa Aesar) had a diameter of 1000 and 500 μm, and a length ranging from 32 to 39 mm. Two pairs of wires were aluminized simultaneously under the same conditions as the nickel foams for times ranging from 10 min to 4 h. The nickel tubes (99.5% purity, from Alfa Aesar) exhibited an outer diameter of 350 μm an inner diameter of 300 μm, and a length ranging from 29 to 36 mm. Aluminization of five tubes per pack was carried out for 2 or 4 h, following the procedures described above, except that the total mass of the pack was reduced to 2 g. Both ends of all tubes were polished to ensure that they were open, thus allowing the ingress of the aluminum halide gases.

2.3. Homogenization treatment

After weighing to record the aluminum mass gain following aluminization, samples were encapsulated in evacuated quartz tubes and annealed at 1273 K for times ranging from 8 to 24 h. Small pieces of Ni_2Al_3 were added to the capsules to prevent aluminum losses during heat-treatment. The phases and compositions of all aluminized and homogenized samples were checked by two or more of the following methods: microbalance weight measurements (±0.3 mg), optical microscopy, Vickers microhardness measurements (100 g load for 15 s), energy dispersive spectroscopy (EDS) in a SEM (±1.2 wt.%), and wet chemical analysis. The EDS profile and Vickers test were calibrated using NiAl, Ni_3Al, Ni_2Al_3, Ni and Al

Table 1
Geometric parameters of nickel foams

Pores per linear inch (ppi)[a]	Foam thickness (mm)	Cell diameter (mm)[b]	Strut width (μm)	Strut wall thickness (μm)	Relative density (%)	Supplier
80	1.6	0.32	54.9±5.0	6.0±1.1	3.5	Goodfellow
20	8.7	1.27	224±34	83.5±21.3	2.2	Astro Met

[a] Data from supplier.
[b] Calculated from ppi value.

standards for which composition was known within 0.01 wt.%.

3. Results

3.1. Nickel tubes and wires

Fig. 1a–c shows optical micrographs of 500 μm diameter nickel wires aluminized for 4 h and subsequently homogenized for 0, 8 or 24 h. Fig. 1a shows the aluminized wire without further heat-treatment, for which only two phases can be clearly identified: a Ni_2Al_3 shell with average thickness of 100 μm and an inner Ni core with average diameter 387 μm; the intermediate NiAl and Ni_3Al layers are too thin to be seen on the micrographs (high magnification observation revealed an irregular NiAl/Ni_3Al layer with thickness of less than 5 μm). The average nickel composition of the wire is about 82 wt.% Ni; thus, after complete homogenization, a two-phase NiAl/Ni_3Al is expected (i.e. an inner core of Ni_3Al and an outer shell of nickel-rich NiAl). Fig. 1b presents the same sample after 8 h of homogenization, where the NiAl/Ni_3Al layer has grown at the expense of the nickel core. Also, there was a significant decrease in the Ni_2Al_3 layer microhardness (from about 700 to about 500 HV), indicating a shift in composition towards NiAl (with hardness 250 HV at stoichiometry), as also observed in Ref. [17]. Fig. 1c shows a sample homogenized for 24 h. Rather than the expected NiAl/Ni_3Al structure described above; the wire consists of a thin irregular outer shell of Ni_2Al_3 in contact with a large inner shell of Al-rich NiAl. These shells are separated by an almost continuous ring of voids from an inner core of nickel.

Fig. 2a shows a nickel tube aluminized for 2 h, with an average nickel composition of 80 wt.%. The structure consists of four concentric shells, with the following compositions (starting from the outside diameter): Ni_2Al_3, NiAl, Ni_3Al and Ni. Most of the porosity is located within the nickel layer and there is no separation of layers by porosity, unlike the situation shown in Fig. 1c. Fig. 2b illustrates a tube homogenized for 10 h after aluminization under the same conditions as Fig. 2a (and with the same composition). Two phases are visible, which, according to the average composition, are expected to be NiAl and Ni_3Al. Most of the porosity within the nickel shell (Fig. 2a) appears to have migrated towards the inner surface of the tube.

3.2. Nickel foams

Fig. 3 gives an overall view of both 80 and 20 ppi foams before and after aluminization. Fig. 3a and b illustrates the cellular structure and the different cell size of the 20 and 80 ppi nickel foams, while Fig. 3c and d depicts the shape, width and wall thickness of the nickel

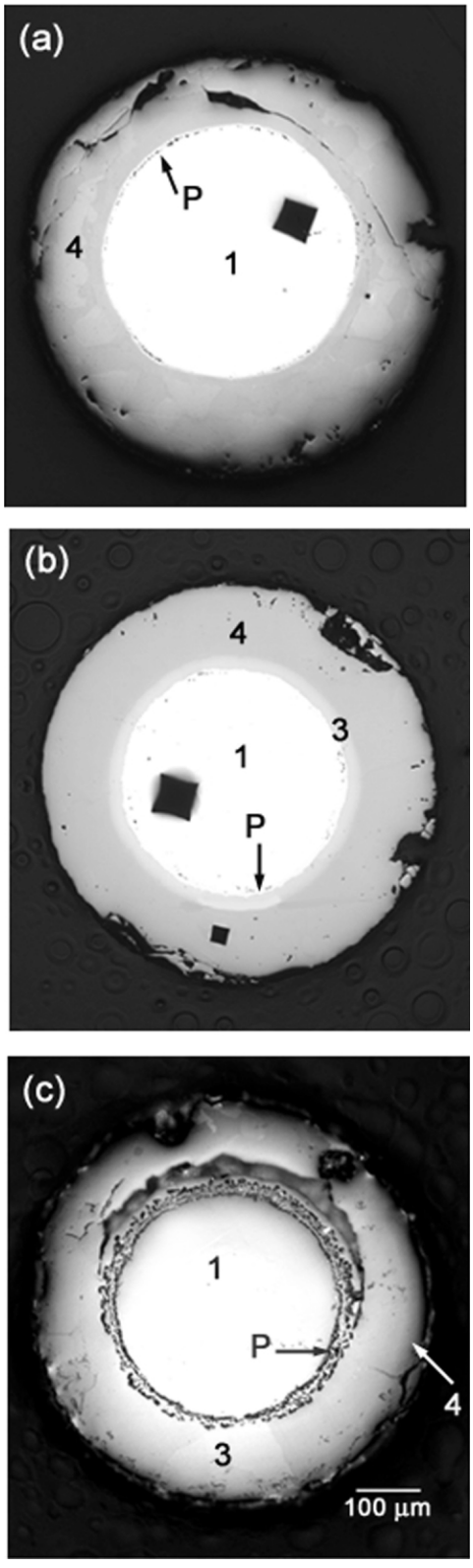

Fig. 1. Optical micrographs of nickel wires (500 μm diameter) aluminized for 4 h (82 wt.% Ni) and homogenized at 1273 K for: (a) 0 h, (b) 8 h and (c) 24 h. Cracks and indentations are due to metallographic preparation and micro-Vickers testing. Phases are labeled as follows—1: Ni, 2: Ni_3Al, 3: NiAl, 4: Ni_2Al_3, P: pores.

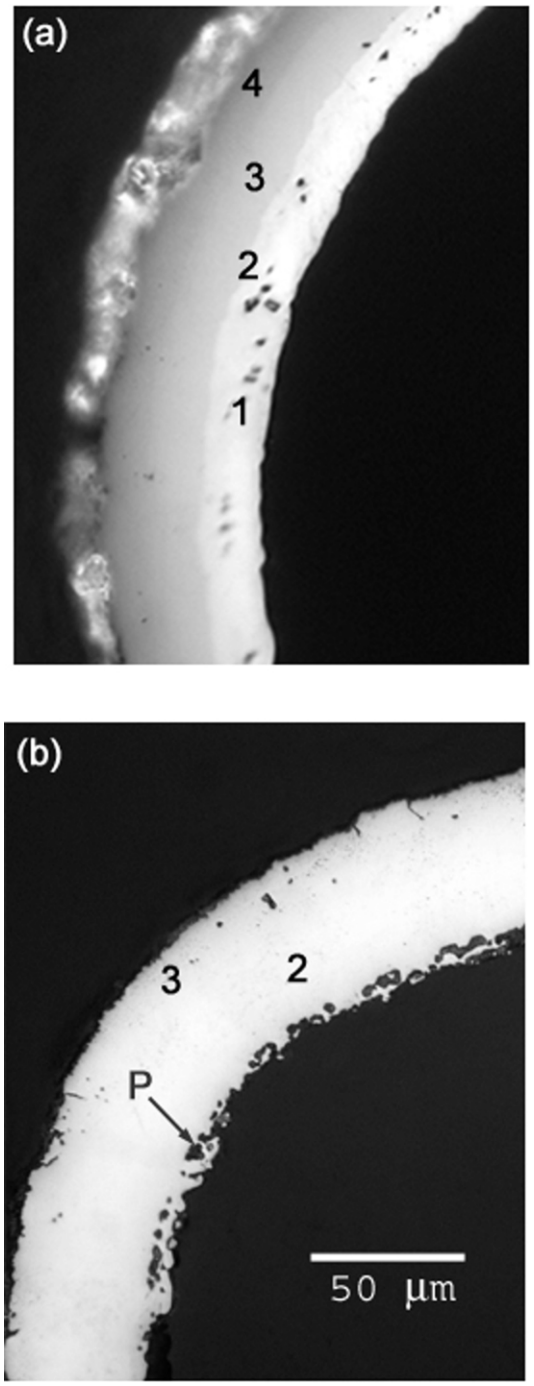

Fig. 2. Optical micrographs of nickel tubes (350 μm outside diameter and 25 μm wall thickness) aluminized for 2 h (80 wt.% Ni) and homogenized for: (a) 0 h and (b) 10 h. Phases are labeled as follows—1: Ni, 2:Ni_3Al, 3: NiAl, 4: Ni_2Al_3, P: pores.

struts (values listed in Table 1), which were fractured to show their hollow structure. Fig. 3e and f, showing both foams after aluminization, demonstrate that the overall foam architecture and the hollow strut morphology are maintained after aluminization; however, a rougher surface topography is observed. All foams conserved their original macroscopic shape and size, as expected if volume increase occurs solely in the radial direction of the struts.

Aluminizing of 80 ppi nickel foams produced a multiphase nickel aluminide structure. Fig. 4a shows an 80 ppi foam aluminized for 0.5 h and with average composition of 78 wt.% Ni (in the NiAl/Ni_3Al two-phase field). The foam wall thickness is 6–14 μm but the plane of polishing is not perpendicular to the strut axis, leading to larger apparent dimensions. The enclosed black areas represent the internal cavities of the hollow struts (visible in Fig. 3c for the nickel foam). In Fig. 4a, the outer surface layer is Ni_2Al_3, which is in contact with a thin layer of NiAl/Ni_3Al next to a Ni core. The same layer sequence is visible from the inner wall surface, indicating that aluminization also occurred from the inner surface of the struts. Fig. 4b shows a foam aluminized for 1.5 h and with an average composition of 68.2 wt.% Ni, close to stoichiometric NiAl. As in Fig. 4a, the outer layer is Ni_2Al_3, followed by a larger NiAl layer and a thin Ni_3Al layer, with some isolated inner Ni regions. Fig. 4c shows the same specimen as in Fig. 4b after 8 h of homogenization. A single NiAl phase is present, with grades of color due to compositional variations within that phase. The average strut wall thickness increased from an initial value of about 6 μm in the initial 80 ppi nickel foam to about 14 μm after 1.5 h of aluminizing. Average grain area, as measured on metallographic sections by optical microscopy, increased from an initial value of 21.2 to 1364 μm^2 after aluminization and subsequent homogenization (corresponding to approximate grain sizes of 5 and 37 μm, respectively). The relative density after homogenization was measured as 7.7%.

Fig. 5a shows the as-received 20 ppi nickel foam, which exhibits significant porosity due to the oxide reduction process used to make the foam. Fig. 5b depicts an aluminized 20 ppi foam with an average composition of 86.3 wt.% Ni (very near stoichiometric Ni_3Al) after 1.5 h of aluminization and homogenized for 10 h, for which two phases can be seen (NiAl/Ni_3Al or Ni/Ni_3Al).

A summary of results from the aluminizing study of foams is presented in Table 2. All but one of the 80 ppi foams have average composition within the broad NiAl phase field (64–76.5 wt.% Ni [15]) and one of the three 80 ppi foams had average composition within the narrow Ni_3Al phase field (85–87 wt.% Ni [15]).

3.3. Aluminization kinetics

Fig. 6 shows the aluminum weight gain (expressed as average aluminum concentration) as a function of aluminization time both wires (500 and 1000 μm diameter) and both foams (20 and 80 ppi). Variations in aluminization kinetics reflect the different surface-to-volume ratios or, equivalently, the different diffusion depths for full aluminization. While the 1000 μm thick wires did

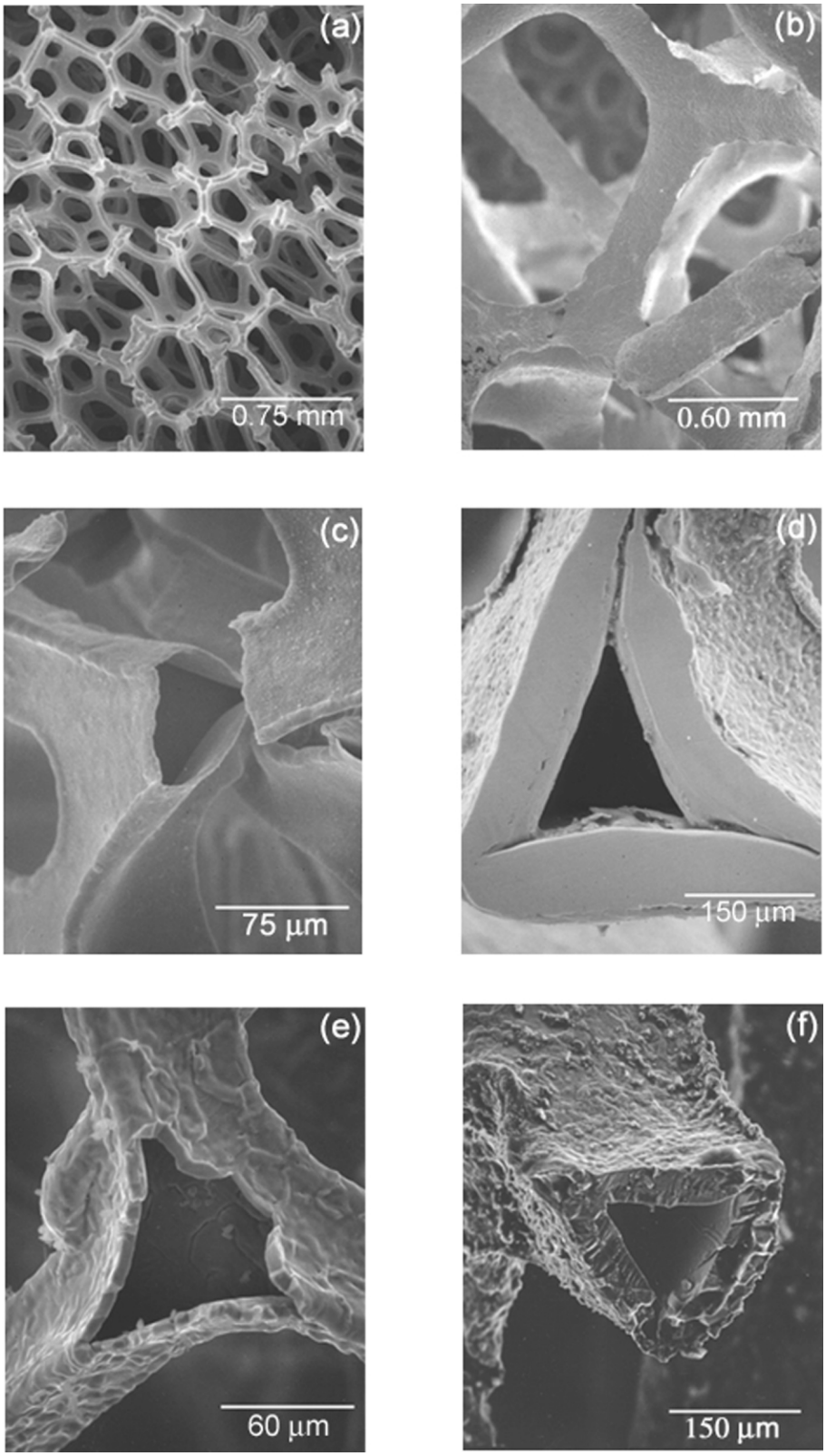

Fig. 3. SEM micrographs of 80 ppi foams (left column) and 20 ppi foams (right column): (a) and (c) as-received 80 ppi foam, (b) and (d) as-received 20 ppi foam and (e) aluminized 80 ppi foam (aluminized 4 h), (f) aluminized 20 ppi foam (aluminized 2 h).

not gain enough aluminum to be homogenized to a single phase, the 500 µm wires gained enough aluminum to display average composition within the Ni_3Al composition after 2 h and within the NiAl–Ni_3Al two-phase field after 4 h of aluminization. The 20 ppi foam with 84 µm wall thickness reached the average Ni_3Al composition

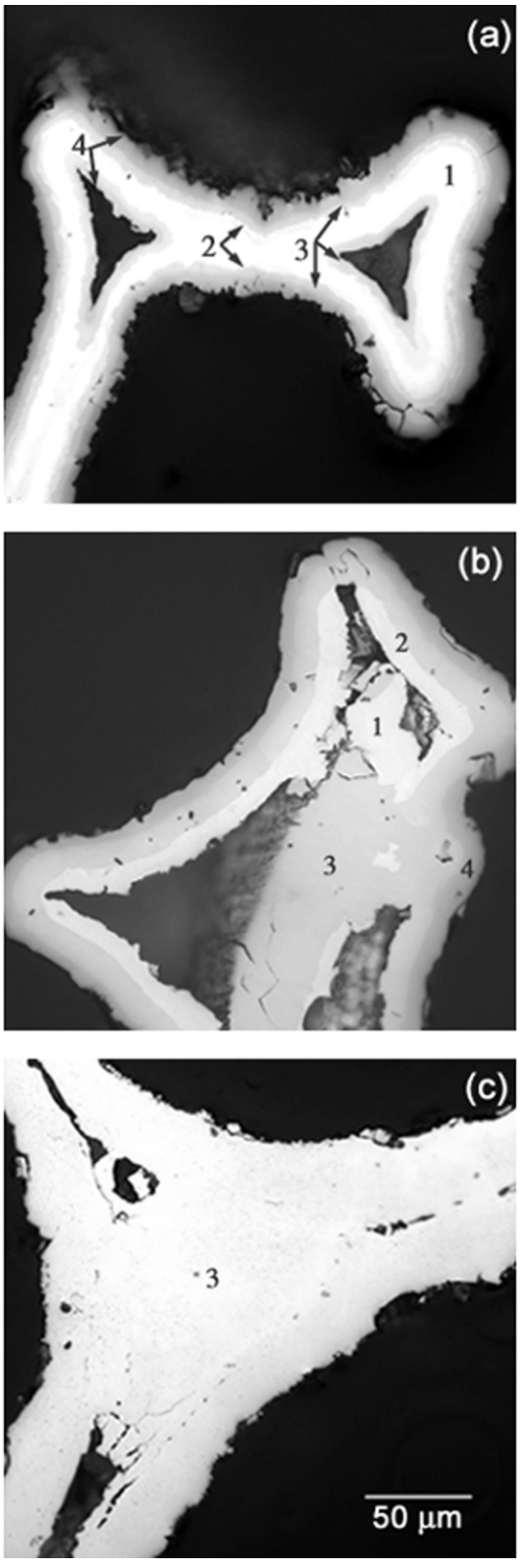

Fig. 4. Optical micrographs of 80 ppi foams: (a) aluminized for 0.5 h (78.0 wt.% Ni), (b) aluminized for 1.5 h (68.2 wt.% Ni), (c) aluminized for 1.5 h (68.2 wt.% Ni) and homogenized for 8 h. Phases are labeled as follows—1: Ni, 2: Ni_3Al, 3: NiAl, 4: Ni_2Al_3.

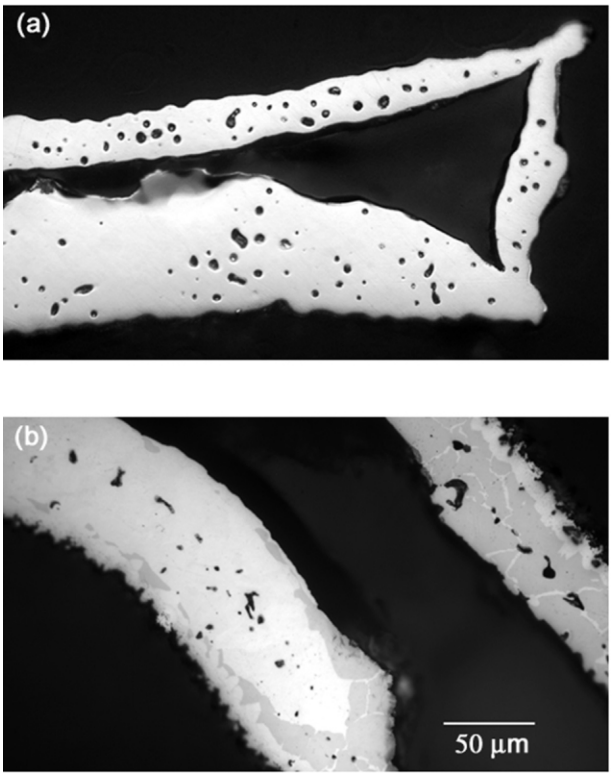

Fig. 5. Optical micrographs of 20 ppi foam: (a) as-received state, showing porosity within struts and (b) after aluminizing for 1.5 h and subsequent homogenization for 10 h (86.3 wt.% Ni), with porosity and two phases.

Table 2
Summary of aluminization and homogenization experiments at 1273 K

Pores per linear inch (ppi)	Aluminizing time (h)	Homogenizing time (h)	Composition (from mass gain) (wt.% Ni)
80	0.5	0	78.4
	1	8	71.9
	1.5	8	66.8 (68.0)[a]
	1.5	8	68.2
	2	0	64.35
20	1.5	10	85.9 (86.3)[a]
	2	8	84.3
	4	0	78.8

[a] From wet chemical analysis.

after 1.5 h of aluminization and could reach stoichiometric NiAl composition after about 19 h (by extrapolation of the best-fit power-law curve). The 80 ppi foam with 6 µm wall thickness showed the fastest Al weight gain, reaching the Ni_3Al composition after about 0.25 h and staying within the NiAl field after 1–2 h of aluminization (stoichiometric NiAl was reached after about 1.5 h).

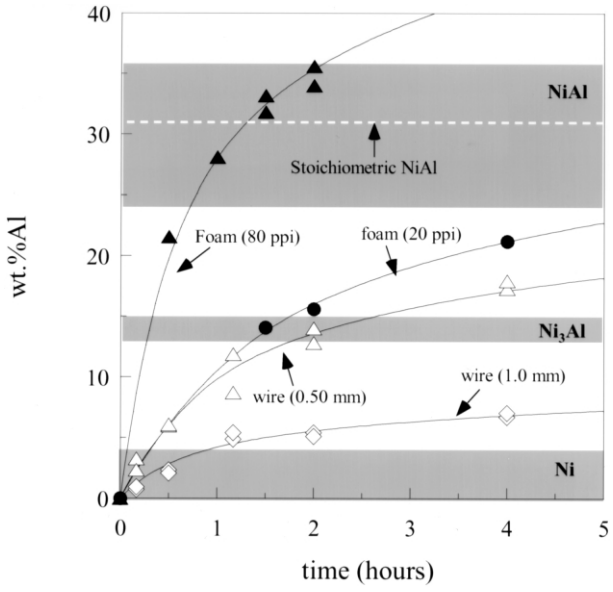

Fig. 6. Time dependence of average composition upon aluminization at 1273 K for 500 and 1000 μm diameter wires and for 20 and 80 ppi foams. Composition ranges of Ni, Ni_3Al and NiAl are shown. Power-law curves are fitted through the data.

4. Discussion

4.1. Phases

Optical micrographs of aluminized nickel rods, tubes and foams (Figs. 1, 2 and 4) revealed a clear contrast between the Ni, NiAl–Ni_3Al and Ni_2Al_3 layers. As reported by other researchers [14,16], the NiAl/Ni_3Al layer was very thin before homogenization, preventing the identification of its individual phases. After heat-treatment, complete homogenization to NiAl was observed for the 80 ppi foam. However, the 20 ppi foam with average Ni_3Al composition did not become a single-phase foam upon homogenization. This is probably due to the large variations in strut thickness (83.5±21.3 μm) in the nickel foam: given a constant aluminum-surface concentration and diffusion time, nickel struts thicker than average will be Al-poor (leading to a Ni–Ni_3Al mixture) and struts thinner than average will be Al-rich (leading to a NiAl–Ni_3Al mixture).

Unlike the tubes, the foams show aluminum deposition taking place from both the inner and outer surfaces of the struts. The lack of aluminum deposition from within the tube despite the open ends, suggest that the halide gases did not penetrate deeply into the long hollow core of the tube (with a length to inner diameter ratio of about 100). The fact that aluminization occurs from within the hollow struts of the foams indicates that there are many openings in the walls of the struts, which were probably created during the removal of the polymer foam after nickel deposition. Ingress of halide gas is thus much easier than for the tubes.

As expected for a diffusion-controlled mechanism, the aluminization kinetics in Fig. 6 shows a power-law time-dependence with exponent less than unity. A simple parabolic behavior is not expected, as the diffusion problem is complicated by the many phases present which lead to large variations in diffusion constants and the presence of moving phase boundaries. Modeling of these results will be addressed in a separate publication [18].

4.2. Volume change

The aluminization of nickel samples leads to a volume increase because of the additional volume taken by the deposited aluminum. For a given sample, the ratio R of the final volume of the intermetallic to the initial volume of the nickel can be expressed as:

$$R = \frac{1}{w_{Ni}} \cdot \frac{\rho_{Ni}}{\rho_{NixAl}} \tag{1}$$

where w_{Ni} is the weight fraction of nickel in the intermetallic, and ρ_{Ni} and ρ_{NixAl} are the density of nickel and the intermetallic phase, respectively. For the formation of stoichiometric NiAl ($\rho_{NiAl} = 5.65$ g/cm^3) and Ni_3Al ($\rho_{Ni3Al} = 7.50$ g/cm^3), the ratio R is 2.30 and 1.37, respectively.

For long wires and tubes, the flux of aluminum and nickel is almost entirely radial, so the volume increase is accommodated by a diameter increase without length change (as observed experimentally in this work). Then the ratio R is:

$$R = \frac{d_o^2 - d_i^2}{d_o'^2 - d_i'^2} \tag{2}$$

where d_o and d_i are the outer and inner diameters of the nickel tube ($d_i = 0$ for a wire), and the prime is used to denote the aluminized state. For the foam, the lack of macroscopic specimen dimension change and the observed radial reaction front within the struts indicate that the volume change is solely accommodated by an increase in strut wall thickness within the foam. Applying Eq. (2) with dimensions given in Table 1 to an aluminized 80 ppi foam, and assuming no internal aluminizing ($d_i = d_i'$) with $R = 2.3$ for stoichiometric NiAl, the calculated increase in wall thickness is about 4.5 μm. Alternately, assuming that all aluminization occurs from the internal surface of the struts ($d_o = d_o'$), the expected increase in wall thickness is about 7.5 μm. This range of 4.5–7.5 μm compare well to the wall thickness increase of 8±2 μm measured on an aluminized 80 ppi specimen with NiAl composition.

The ratio R also represents the factor by which the relative density of the foam increases after aluminization, provided the macroscopic dimensions of the foam specimen are unchanged, as observed in the present

study. For example, the 80 ppi nickel foams (with initial relative density of 3.5%) are predicted to exhibit a relative density of 8.1% after aluminization to stoichiometric NiAl, in good agreement with the measured value of 7.7% (the calculated porosity over the whole composition range of NiAl ranges from 7 to 10%). The 20 ppi nickel foams (with initial relative density of 2.2%) homogenized to Ni_3Al composition is predicted to show a relative density of 3.0%.

4.3. Porosity

Voids in the partially aluminized nickel wires and tubes are due to the Kirkendall effect, which is pronounced in the Ni–Al system [17]. Their coalescence separated the outer Al-rich shells from the inner Ni-rich core, thus preventing global equilibrium upon homogenization. A similar effect was observed in Ref. [19], where an infiltrated material consisting of individual nickel spheres within an aluminum-rich matrix was annealed at 1473 K: intermetallic formation initially took place by interdiffusion between the matrix and the spheres, but the diffusion flux was prematurely interrupted by the formation of Kirkendall-induced gaps separating completely the spheres from the matrix. In our case, each region can however be single phase and free of concentration gradients after homogenization, since the Ni and the NiAl phases have large solubilities for Al and Ni, respectively. Furthermore, Fig. 1c illustrates that for the aluminization conditions used here, wires with at most $\sim$100 μm radius can be aluminized and homogenized to form NiAl. Aluminization for higher depths may require different homogenization temperatures or an intermediate pore densification step. The single-step aluminization process described by Das et al. [13] could also solve the porosity problem caused by homogenization of Ni_2Al_3, since that process produces NiAl as the main phase, with little or no expected Kirkendall porosity.

It follows from the above experiments that tubes (or, for foams, hollow struts) with wall thickness less than about 100 μm should be amenable to full aluminization to NiAl: assuming aluminization from the outer surface only, Kirkendall pores migrating with the Ni_3Al/Ni interface will disappear at the inner surface of the tube or strut, before they can coalesce into a circumferential gap preventing diffusion as in Fig. 1c. Fig. 2b supports this prediction, as it shows that nickel tubes with 25 μm wall thickness exhibited Kirkendall pores located at the inner surface of the tube. In contrast, the 80 ppi nickel foam for which aluminizing was taking place from both the inner and outer surfaces of the hollow foam strut is expected to show Kirkendall porosity midway within the wall thickness of the strut, where the last nickel region exists (Fig. 4a). The observed lack of porosity (Fig. 4c) can be explained by the very thin strut wall thickness (6 μm) preventing the accumulation of significant Kirkendall pore volume.

Another source of porosity originates from the as-processed 20 ppi nickel foam (Fig. 5a). While these pores may shrink during aluminization by sintering and by the addition of aluminum, they may also grow by incorporating Kirkendall vacancies during the subsequent homogenization to NiAl. Fig. 5b shows no significant differences in pore size and volume fraction in the 20 ppi foam with average Ni_3Al composition, most probably because the Kirkendall effect is not as pronounced as for the NiAl composition.

4.4. Aluminide foams for high-temperature applications

The present results demonstrate that pack-aluminization followed by homogenization, is a simple method to synthesize nickel–aluminide foams. The process maintains the highly-structured, complex geometry of the nickel foam (hollow struts, open cells) while increasing the foam relative density by a factor of 1.4–2.3 for Ni_3Al and NiAl. Nickel–aluminide foams with different architectures and porosities should be amenable to fabrication by this new process. Also, additional alloying elements (e.g. boron in Ni_3Al or zirconium in NiAl [20,21]) could be added by diffusion before, during or after aluminization and homogenization. The process can further be applied to produce foams of other technologically-relevant aluminides (e.g. iron, cobalt, titanium, platinum and ruthenium).

Two limitations preventing full aluminization are apparent for the conditions studied here. First, Kirkendall pores accumulate at the moving Ni/Ni_3Al boundary and coalesce into large gaps preventing mass flow for aluminization depths greater than about 100 μm. Thus, the largest wall thickness of foams which can be fully aluminized is about 100 μm, or twice this amount if aluminization can occur from within the hollow strut. Second, local variations in strut wall thickness lead to corresponding variations in composition, which over short ranges can be smoothed by homogenization. For NiAl, these composition variations are usually less significant, as this phase has a broad range of composition over which creep properties do not vary significantly. For foams with target compositions of Ni_3Al, however, the narrow range in which Ni_3Al exists will lead to two-phase regions (Ni/Ni_3Al or NiAl/Ni_3Al) where the strut wall thickness deviates from average. Even though the strut thickness deviation problem could be solved by using nickel foams made by CVD which gives a very uniform thickness, the CVD process itself significantly limits the maximum foam strut thickness as well as the maximum macroscopic dimension of the foam. Another route to fabricate a nickel foam with no variation in strut thickness is to use nickel wires or tubes of uniform diameters. Cellular nickel structures can then be produced by

standard techniques used to make ceramic fiber preforms (pressing of chopped fibers, stacking of woven fabrics or 3D weaving of continuous fibers), lightly pre-sintered if necessary, and finally aluminized as discussed in the present paper. We finish this discussion by noting that full aluminization of the nickel foams may not be desirable in all cases. For instance, a partially-aluminized foam with an outer strut surface consisting of oxidation- and corrosion resistant nickel aluminides and an inner strut region of tough nickel (or nickel alloy) may have better structural performance than a single-phase aluminide foams.

5. Conclusions

The pack-aluminizing process used to create aluminide coatings on the surface of nickel and nickel-base alloys has been used to synthesize nickel aluminide foams from commercially-available nickel foams with 96–98% porosity. Using a high-activity pack, 80 and 20 ppi nickel foams were aluminized at 1273 K for times ranging from 0.5 to 4 h; after aluminization the foams presented a range of aluminide phases, which were subjected to a subsequent homogenization treatment at 1273 K. This resulted in a single-phase NiAl structure for 80 ppi foams, but single-phase Ni_3Al foams could not be produced from 20 ppi nickel foams, due to the narrow range of solubility in this phase and the broad range of wall thickness in the original nickel foam.

Acknowledgements

Financial support in the form of an NSF Graduate Fellowship for A.M.H. is acknowledged. We thank David Levine from Astro Met for providing some of the nickel foams used in this study, as well as Dr. Michael Nathal from the NASA Glenn Center and Christopher Schuh from Northwestern University for useful discussions.

References

[1] Davies GJ, Zhen S. J Mater Sci 1983;18:1899.
[2] Darolia R. Intermetallics 2000;8:1321.
[3] Stoloff NS, Liu CT. In: Stoloff NS, Sikka VK, editors. Physical metallurgy and processing of intermetallic compounds. New York: Chapman & Hall, 1996, p. 159.
[4] Noebe RD, Bowman RR, Nathal MV. Int Mater Rev 1993; 38:193.
[5] Chung HS, Park GP, Lim JH, Kim K, Lee JK, Moon KH, Youn JH. J Power Sources 1998;49:3109.
[6] Dunand DC. Mater Manuf Proc 1995;10(3):373.
[7] Hickl AJ, Heckel RW. Metall Mater Trans 1975;6A:431.
[8] Kim S, Chang YA. Metall Mater Trans 2000;31A:1519.
[9] Rairden JR, Jackson MR. J Vac Sci Technol 1980;17(1):77.
[10] Levine SR, Caves RM. J Electrochem Soc 1974;121(8):1051.
[11] Levine D. (Astro Met), personal communication.
[12] Badiche X, Forest S, Guibert T, Bienvenu Y, Bartout J-D, Ienny P, Croset M, Bernet H. Mater Sci Eng 2000;289A:276.
[13] Das DK, Singh V, Joshi SV. Metall Mater Trans 1998;29A:2173.
[14] Jansen MMP, Rieck GD. Trans TMS-AIME 1967;239:1372.
[15] Nash P, Singleton MF, Murray JL. In: Nash P, editor. Phase diagrams of binary alloys, vol. 1. Ohio, ASM International, 1991. p. 311.
[16] Goward GW, Boone DH, Giggins CS. Trans ASM 1967;60:228.
[17] Jansen MMP. Metall Trans 1973;4:1623.
[18] Hodge AM, Schuh C, Dunand DC. Manuscript in preparation.
[19] Dunand DC. J Mater Sci 1994;29:4056.
[20] Whittenberger JD, Noebe RD. Metall Mater Trans 1996; 27A:2628.
[21] George EP, Liu CT. J Mater Res 1990;5:754.